

Quantum Embedding Theory for Strongly-correlated States in Materials

He Ma,[†] Nan Sheng,[†] Marco Govoni,^{*,‡,¶} and Giulia Galli^{*,‡,†,¶}

[†]*Department of Chemistry, University of Chicago, Chicago, IL 60637, USA.*

[‡]*Pritzker School of Molecular Engineering, University of Chicago, Chicago, IL 60637, USA.*

[¶]*Materials Science Division and Center for Molecular Engineering, Argonne National Laboratory, Lemont, IL 60439, USA.*

E-mail: mgovoni@anl.gov; gagalli@uchicago.edu

Abstract

Quantum embedding theories are promising approaches to investigate strongly-correlated electronic states of active regions of large-scale molecular or condensed systems. Notable examples are spin defects in semiconductors and insulators. We present a detailed derivation of a quantum embedding theory recently introduced, which is based on the definition of effective Hamiltonians. The effect of the environment on a chosen active space is accounted for through screened Coulomb interactions evaluated using density functional theory. Importantly, the random phase approximation is not required and the evaluation of virtual electronic orbitals is circumvented with algorithms previously developed in the context of calculations based on many-body perturbation theory. In addition, we generalize the quantum embedding theory to active spaces composed of orbitals that are not eigenstates of Kohn-Sham Hamiltonians. Finally, we report results for spin defects in semiconductors.

1 Introduction

Atomistic, quantum mechanical simulations are playing an increasingly important role in designing functional materials. In the past three decades, density functional theory (DFT) has become a standard method for quantum mechanical simulations of molecules and condensed systems. While DFT has been successfully applied to predict structural and electronic properties of a variety of systems at zero and finite temperature, DFT calculations do not accurately describe strongly-correlated electronic states, i.e. states that cannot be represented by a single determinant of one-electron orbitals.^{1,2} Prominent examples of strongly-correlated systems include transition metal oxides with localized *d* or *f* bands,³ deep centers in semiconductors,⁴ and reactions centers in enzymes.^{5,6} Developing efficient and accurate methods to simulate strongly-correlated electronic states is a long-standing challenge for the electronic structure community.

In principle, any electronic state, whether strongly or weakly correlated, can be described by performing full configuration-interaction (FCI) calculations, which exactly solve the many-body Schrödinger equation of electrons subject to the potential of the surrounding nuclei. However, the computational cost of FCI calculations grows exponentially as the system size increases (the curse of dimensionality). Sophisticated methods have been developed to approximately solve the many-body Schrödinger equation and to provide insight into strongly-correlated electronic states, such as dynamical mean-field theory,^{7,8} quantum Monte-Carlo^{9,10} and various multi-reference quantum chemistry methods.¹¹ These approaches are in general much more computationally demanding than DFT.

Quantum embedding theories are promising approaches to study strongly-correlated states in materials because they enable the use of high-level theories for selected degrees of freedom of the system (defined by a chosen active space) while treating the rest of the system (environment) within mean-field theories. Various embedding schemes have been proposed based on different fundamental quantities,¹² such as the electron density,^{13–18} density matrix^{19–21} and Green’s function.^{22–32} In this work, we focus on a quantum embedding

theory based on the screened Coulomb interactions, with the goal of developing an approach scalable to large systems, with hundreds of atoms. The method is inspired by the constrained random phase approximation (cRPA),²⁵ which has been used to construct effective Hamiltonians acting on selected energy bands (active space) in complex materials, such as oxides,^{33–36} 2D materials,³⁷ and spin-defects in wide-gap semiconductors.⁴ Two approximations are usually adopted to evaluate the dielectric screening in cRPA calculations: (i) the random phase approximation (RPA), which neglects the exchange-correlation interaction between electrons in evaluating the dielectric screening,³⁸ thus affecting the accuracy of the calculation; (ii) the Adler-Wiser formalism^{39,40} that involves explicit summations over empty states, thus affecting the efficiency of calculations. Recently, we developed a quantum embedding theory that overcomes both approximations:⁴¹ the dielectric screening is computed beyond the RPA by including exchange-correlation effects evaluated using a finite-field algorithm,^{42,43} and the summation over empty states is circumvented by using a compact basis obtained through the spectral decomposition of density response functions.^{44–47} We applied the embedding theory to study several spin-defects in semiconductors relevant for quantum information technologies,^{41,48} and we demonstrated that the theory can accurately predict the excitation energies for strongly-correlated excited states.

In this work, we present a detailed derivation of the quantum embedding theory introduced in Ref. 41, and we discuss the accuracy of several strategies to compute the dielectric screening of the environment beyond the random phase approximation (RPA). Using spin-defects as examples, we show that the most accurate results are obtained by properly including in the calculation the exchange-correlation effects of the environment without double counting exchange-correlation effects in the active space. We further extend the quantum embedding formalism to cases where the embedding is achieved by using projection operators that do not commute with the Kohn-Sham Hamiltonian. The generalized formulation is thus not restricted to the use of Kohn-Sham orbitals to define active spaces, but allows as well for the use of localized orbitals, e.g. maximally localized Wannier functions (MLWFs).⁴⁹ We

report proof-of-principles calculations of spin-defects and of a transition metal oxide, SrTiO₃ using active spaces defined with MLWFs.

The rest of the paper is organized as follows. In Sec. 2 we describe the formalism of the quantum embedding theory within and beyond the RPA description of dielectric screening, and we discuss how quantum embedding calculations can be performed without explicit summation over empty states. In Sec. 3 we present benchmark calculations on spin-defects and SrTiO₃. Sec. 4 contains our summary and conclusions.

2 Methods

In the following discussion, we will focus on systems represented by large periodic cells for which only the Γ point is required to sample the Brillouin zone.

2.1 Effective Hamiltonian and cRPA embedding

Under the Born-Oppenheimer and nonrelativistic approximations, the many-body Hamiltonian of a system of interacting electrons is

$$H = \sum_{ij} t_{ij} a_i^\dagger a_j + \frac{1}{2} \sum_{ijkl} v_{ijkl} a_i^\dagger a_j^\dagger a_l a_k \quad (1)$$

where a^\dagger and a are creation and annihilation operators acting on single-electron states i, j, k, l ; the one-electron term t includes the kinetic energy and the electron-nuclei interaction; the two-electron term v represents the *bare* Coulomb interaction between electrons. The exact diagonalization of H can only be carried out for small systems due to the high computational cost.

If electronic excitations of interest occur within a small subspace (denoted as the active space A) of the full Hilbert space, then a quantum embedding scheme may be used to

construct an effective Hamiltonian, H^{eff} , that acts only on the active space:

$$H^{\text{eff}} = \sum_{ij}^{\text{A}} t_{ij}^{\text{eff}} a_i^\dagger a_j + \frac{1}{2} \sum_{ijkl}^{\text{A}} v_{ijkl}^{\text{eff}} a_i^\dagger a_j^\dagger a_l a_k \quad (2)$$

where t^{eff} and v^{eff} are renormalized one-electron and two-electron terms that take into account the interactions between the active space and the environment. The parameters of the effective Hamiltonian may be determined by fitting experimental results or may be derived from first-principles calculations. In this work we determine the parameters of the effective Hamiltonian using DFT calculations. We note again that the form of the effective Hamiltonian is general and may reduce to that of the Hubbard model if certain terms are excluded from the summations entering Eq. 2, indicating that first-principles calculations of v_{ijkl}^{eff} may be used to obtain Hubbard parameters (e.g., U)²⁵ for DFT+U calculations,^{3,50} as discussed later in the paper.

Within DFT, a mean-field description of the full system is obtained by solving self-consistently the Kohn-Sham equations

$$H_{\text{KS}} \psi_m(\mathbf{x}) = \varepsilon_m \psi_m(\mathbf{x}), \quad (3)$$

where the Kohn-Sham Hamiltonian $H_{\text{KS}} = T + V_{\text{SCF}} = T + V_{\text{ion}} + V_{\text{H}} + V_{\text{xc}}$; T is the kinetic energy operator; V_{SCF} is the KS potential that includes the ionic V_{ion} , the Hartree V_{H} and the exchange-correlation potential V_{xc} ; m is the index for Kohn-Sham (spin-)orbitals $\psi_m(\mathbf{x})$. $\mathbf{x} = (\mathbf{r}, \sigma)$ where \mathbf{r} and σ are electron coordinate and spin, respectively. Within linear response, we define the Kohn-Sham polarizability $\chi_0(\mathbf{x}_1, \mathbf{x}_2, \omega)$ that represents the response of the electronic density at \mathbf{x}_1 caused by a monochromatic perturbative potential exerted at

\mathbf{x}_2 with frequency ω :

$$\chi_0(\mathbf{x}_1, \mathbf{x}_2, \omega) = \sum_i^{\text{occ}} \sum_j^{\text{emp}} \psi_i(\mathbf{x}_1) \psi_j(\mathbf{x}_1) \psi_j(\mathbf{x}_2) \psi_i(\mathbf{x}_2) \left\{ \frac{1}{\omega - (\varepsilon_j - \varepsilon_i) + i\eta} - \frac{1}{\omega + (\varepsilon_j - \varepsilon_i) - i\eta} \right\} \quad (4)$$

where “occ” and “emp” denote summation over occupied and empty (virtual) Kohn-Sham orbitals, respectively; η is a infinitesimal positive value. Similar to the derivation of the GW method within many-body perturbation theory,⁵¹ one can use the polarizability to define the screened Coulomb interaction W of the system. Within the RPA, W can be computed through a Dyson equation:

$$W_{\text{rpa}} = v + v\chi_0 W_{\text{rpa}} \quad (5)$$

where v is the bare Coulomb interaction.

In the cRPA approach, the two-body term of the effective Hamiltonian, v^{eff} , is computed as a partially screened Coulomb interaction

$$W_{\text{rpa}}^{\text{E}} = v + v\chi_0^{\text{E}} W_{\text{rpa}}^{\text{E}} \quad (6)$$

where E denotes the environment and $\chi_0^{\text{E}} = \chi_0 - \chi_0^{\text{A}}$. χ_0^{A} is the Kohn-Sham polarizability projected onto an active space⁵²

$$\chi_0^{\text{A}}(\mathbf{x}_1, \mathbf{x}_2, \omega) = \sum_i^{\text{occ}} \sum_j^{\text{emp}} (O^{\text{A}}\psi_i)(\mathbf{x}_1) (O^{\text{A}}\psi_j)(\mathbf{x}_1) \psi_j(\mathbf{x}_2) \psi_i(\mathbf{x}_2) \left\{ \frac{1}{\omega - (\varepsilon_j - \varepsilon_i) + i\eta} - \frac{1}{\omega + (\varepsilon_j - \varepsilon_i) - i\eta} \right\} \quad (7)$$

where we defined the projector into the active space as $O^{\text{A}} = \sum_i^{\text{A}} |\zeta_i\rangle \langle \zeta_i|$, and ζ_i are orthogonal orbitals spanning the active space.

If the active space is spanned by a set of Kohn-Sham orbitals, χ_0^{A} can be evaluated using a similar summation-over-state expression as Eq. 4, with summations limited to Kohn-Sham

orbitals in the active space A only:

$$\chi_0^A(\mathbf{x}_1, \mathbf{x}_2, \omega) = \sum_{i \in A}^{\text{occ}} \sum_{j \in A}^{\text{emp}} \psi_i(\mathbf{x}_1) \psi_j(\mathbf{x}_1) \psi_j(\mathbf{x}_2) \psi_i(\mathbf{x}_2) \left\{ \frac{1}{\omega - (\varepsilon_j - \varepsilon_i) + i\eta} - \frac{1}{\omega + (\varepsilon_j - \varepsilon_i) - i\eta} \right\} \quad (8)$$

We note that $W_{\text{rpa}}^{\text{E}}$ represents the effective interaction between electrons considering only the screening of the environment, characterized by χ_0^{E} ; the full W_{rpa} may be recovered by adding to $W_{\text{rpa}}^{\text{E}}$ the screening of the active space

$$W_{\text{rpa}} = W_{\text{rpa}}^{\text{E}} + W_{\text{rpa}}^{\text{E}} \chi_0^A W_{\text{rpa}} \quad (9)$$

The two-body term v^{eff} in the effective Hamiltonian (Eq. 2) may be computed as

$$v_{ijkl}^{\text{eff}} = \int d\mathbf{x} d\mathbf{x}' \zeta_i(\mathbf{x}) \zeta_k(\mathbf{x}) W_{\text{rpa}}^{\text{E}}(\mathbf{x}, \mathbf{x}') \zeta_j(\mathbf{x}') \zeta_l(\mathbf{x}') \quad (10)$$

As we discuss in Sec. 2.2, v^{eff} may be evaluated beyond the RPA, and calculations may be performed with general definitions of active spaces, without explicit summations over empty states (see Sec. 2.3).

Once v^{eff} is obtained, the one-body term t^{eff} entering Eq. 2 may be computed by subtracting from the Kohn-Sham Hamiltonian a term that accounts for electrostatic and exchange-correlation interactions in the active space^{4,41}

$$t_{ij}^{\text{eff}} = H_{ij}^{\text{KS}} - \left(\sum_{kl} v_{ikjl}^{\text{eff}} \rho_{kl} - \sum_{kl} v_{ijkl}^{\text{eff}} \rho_{kl} \right) \quad (11)$$

where $\rho_{ij} = \sum_m^{\text{occ}} \langle \zeta_i | \psi_m \rangle \langle \psi_m | \zeta_j \rangle$ is the one-electron reduced density matrix. We remark that the strategy used in Eq. 11 to remove double counting is similar to the fully-localized limit (FLL) scheme^{53,54} that is widely used in DFT+U calculations for treating double counting of interaction energies within d or f shells.

2.2 Screened Coulomb interaction beyond the RPA

In this section we consider several definitions of partially screened Coulomb interaction W^E beyond the RPA. Within many-body perturbation theory, two common expressions⁵⁵ of the screened Coulomb interaction beyond RPA are defined, depending on whether the interacting charges are excluded from or included in the self-consistent solution of the Kohn-Sham system. The two definitions are called test-charge W (W_{tc}) and test-electron W (W_{el}), respectively.^{56–58}

$$W_{tc} = v + vPW_{tc} \quad (12)$$

$$W_{el} = f_{Hxc} + f_{Hxc}\chi_0 W_{el} \quad (13)$$

where the irreducible polarizability P is defined as the derivative of the electron density with respect to the classical electrostatic potential V_{cl} (the sum of Hartree and external potential): $P = \frac{\delta n}{\delta V_{cl}} = \chi_0 + \chi_0 f_{xc} P$; the Hartree-exchange-correlation kernel f_{Hxc} is defined as $f_{Hxc} = v + f_{xc}$, where the exchange-correlation kernel f_{xc} is the functional derivative of V_{xc} with respect to the density $f_{xc} = \frac{\delta V_{xc}}{\delta n}$. W_{tc} and W_{el} are adopted in many-body perturbation theory calculations of quasiparticle energies and electron-phonon coupling beyond the RPA.^{42,57,59–62} W_{tc} and W_{el} both reduce to W_{rpa} when the RPA is invoked, i.e. when $f_{xc} = 0$.

Inspired by the cRPA formalism, we define partially screened test-charge and test-electron Coulomb interactions (W_{tc}^E and W_{el}^E , respectively). To this end, we partition the irreducible polarizability $P = P^A + P^E$ and the Kohn-Sham polarizability $\chi_0 = \chi_0^A + \chi_0^E$ into contributions from the active space and the environment, where χ_0^A is defined in Eq. 7. We define P^A as $P^A = \chi_0^A + \chi_0^A f_{xc} P^A$, and W_{tc}^E and W_{el}^E as:

$$W_{tc}^E = v + vP^E W_{tc}^E \quad (14)$$

$$W_{el}^E = f_{Hxc} + f_{Hxc}\chi_0^E W_{el}^E \quad (15)$$

The quantities W_{tc}^E and W_{el}^E defined above have the property that the corresponding full

W can be obtained by further screening W^E with χ_0^A or P^A , similar to the cRPA formulation (Eq. 9):

$$W_{tc} = W_{tc}^E + W_{tc}^E P^A W_{tc} \quad (16)$$

$$W_{el} = W_{el}^E + W_{el}^E \chi_0^A W_{el} \quad (17)$$

We note that neither W_{tc}^E nor W_{el}^E shall be used as the effective electron interactions v^{eff} beyond the RPA in the definition of the effective Hamiltonian. If $v^{\text{eff}} = W_{tc}^E$, then electrons in the active space interact with electrons in the environment through the bare Coulomb interaction, and the exchange-correlation effects between electrons in the active space and the environment are not correctly included. If $v^{\text{eff}} = W_{el}^E$, then the exchange-correlation effects are double-counted when diagonalizing the effective Hamiltonian, since the exchange-correlation effects between electrons in the active space are already accounted for through the f_{xc} term entering the bare part of W_{el}^E . Hence, based on physical considerations, we propose to use $v^{\text{eff}} = W_{\text{vel}}$, where we define W_{vel} as the sum of the bare Coulomb interaction v and the polarization part (second term in r.h.s. of Eq. 15) of W_{el} :

$$W_{\text{vel}}^E = v + f_{\text{Hxc}} \chi_0^E W_{el}^E \quad (18)$$

W_{vel}^E includes exchange-correlation effects in the environment while avoiding the double counting of exchange-correlation effects in the active space (see also the Supporting Information (SI) of Ref. 41). In Sec. 3.2 we perform quantum embedding calculations of spin-defects in semiconductors with effective interactions defined as W_{rpa}^E , W_{tc}^E , W_{el}^E and W_{vel}^E , and we demonstrate that effective Hamiltonians constructed from W_{vel}^E indeed lead to accurate predictions of excitation energies of spin-defects. To summarize the formalism described in this section, in Fig. 1 we present a comparison of quantum embedding calculation workflows within and beyond the RPA using W_{rpa}^E and W_{vel}^E , respectively.

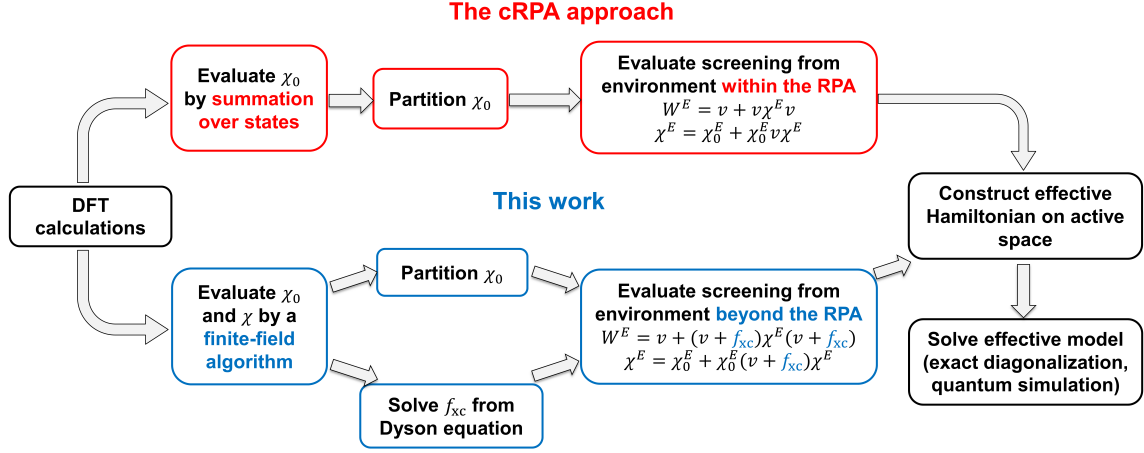


Figure 1: Comparison of workflows for quantum embedding calculations within and beyond the random phase approximation.

2.3 Evaluation of W^E without empty states

In this section we discuss how to evaluate W^E without explicitly computing virtual electronic states, by representing χ_0 on a compact basis. The formalism discussed in this subsection is general and is applicable regardless of whether the active space is defined using eigenstates of the Kohn-Sham Hamiltonian.

We consider the spin-unresolved $\chi_0(\mathbf{r}, \mathbf{r}')$, where the spin index is already summed over. We use a so-called projected-dielectric eigendecomposition (PDEP) basis,^{44–47} obtained by the spectral decomposition of the symmetrized Kohn-Sham polarizability $\tilde{\chi}_0 = v_c^{\frac{1}{2}} \chi_0 v_c^{\frac{1}{2}}$ at zero frequency. To obtain the PDEP basis, we use the Davidson algorithm to compute N_{PDEP} eigenvectors of $\tilde{\chi}_0(\omega = 0)$ with the most negative eigenvalues:

$$\tilde{\chi}_0(\omega = 0) \approx \sum_i^{N_{\text{PDEP}}} \lambda_i |\varphi_i\rangle \langle \varphi_i| \quad (19)$$

The accuracy of response functions and screened Coulomb interactions are thus determined

by the parameter N_{PDEP} used in Eq. 19, and in the SI we show, as examples, the rapid convergence of excitation energies of spin-defects and Hubbard parameters of SrTiO_3 as functions of N_{PDEP} .

We use a finite-field algorithm^{42,43} to evaluate the matrix elements of the symmetrized static reducible polarizability $\tilde{\chi} = \tilde{\chi}_0 + \tilde{\chi}_0 \tilde{f}_{\text{Hxc}} \tilde{\chi}$ on the PDEP basis, where $\tilde{f}_{\text{Hxc}} = v_c^{-\frac{1}{2}} f_{\text{Hxc}} v_c^{-\frac{1}{2}}$. In the finite-field algorithm, one evaluates the charge density ρ_i^\pm of the Kohn-Sham system subject to the perturbation $\tilde{\varphi}_i = v_c^{\frac{1}{2}} \varphi_i$ by solving the Kohn-Sham equations with $H^{\text{KS}} \pm \tilde{\varphi}_i$. Then one can compute the linear variation of the electronic density using central finite differences, i.e., $\Delta\rho_i = \frac{\rho_i^+ - \rho_i^-}{2}$. The matrix elements of $\tilde{\chi}$ in the PDEP basis are therefore given by:

$$\tilde{\chi}_{ij} = \langle \tilde{\varphi}_i | \Delta\rho_j \rangle \quad (20)$$

We note that all potential terms within the Kohn-Sham Hamiltonian are updated during the self-consistent iterations.^{42,43} We then compute the matrix elements of \tilde{f}_{xc} using the following matrix identity:

$$\tilde{f}_{\text{xc}} = \tilde{\chi}_0^{-1} - \tilde{\chi}^{-1} - 1. \quad (21)$$

The matrix inversion operations entering Eq. 21 is efficiently carried out using the PDEP compact basis set, where $N_{\text{PDEP}} \ll N_{\text{PW}}$ (the number of plane-wave basis functions).

At arbitrary frequency, the matrix elements of $\tilde{\chi}_0$ on the PDEP basis can be computed as⁴⁷

$$\tilde{\chi}_{0ij}(\omega) = \sum_n^{\text{occ}} \langle \xi_n^i | O^c \left[(\varepsilon_n - H_{\text{KS}} - \omega + i\eta)^{-1} + (\varepsilon_n - H_{\text{KS}} + \omega + i\eta)^{-1} \right] O^c | \xi_n^j \rangle \quad (22)$$

where i, j are indices for PDEP basis functions, and $\xi_n^i(\mathbf{r}) = \tilde{\varphi}_i(\mathbf{r})\psi_n(\mathbf{r})$, where $\psi_n(\mathbf{r})$ denotes the spatial part of the Kohn-Sham orbital $\psi_n(\mathbf{x})$. The summation over empty states in Eq. 4 is formally replaced by the projection operator O^c onto virtual manifold. In practical calculations, O^c is replaced with $1 - O^v$, where O^v is the projection onto the occupied

manifold. Thus Eq. 22 can be evaluated without explicitly summing over empty states. Furthermore, the frequency dependence of χ_0 can be efficiently included through the use of the Lanczos algorithm,⁴⁷ although in this work we only consider zero frequency response functions and we do not further investigate their frequency dependence.

Similar to Eq. 22, $\tilde{\chi}_0^A$ can be written as

$$\tilde{\chi}_{0ij}^A(\omega) = \sum_n^{\text{occ}} \langle \xi_n^{Ai} | O^A O^c \left[(\varepsilon_n - H_{\text{KS}} - \omega + i\eta)^{-1} + (\varepsilon_n - H_{\text{KS}} + \omega + i\eta)^{-1} \right] O^c | \xi_n^j \rangle \quad (23)$$

where $\xi_n^{Ai}(\mathbf{r}) = \tilde{\varphi}_i(\mathbf{r})(O^A \psi_n)(\mathbf{r})$. Therefore, $\tilde{\chi}_0^A$ at zero or finite frequency can be evaluated in a similar manner as $\tilde{\chi}_0$, i.e., without explicit summation over empty states. We note that Eq. 23 does not assume that the active space is defined through a set of Kohn-Sham orbitals (i.e. we do not assume that O^A commutes with H^{KS}).

Once $\tilde{\chi}_0^A$ is evaluated, we can compute a set of partial reducible polarizabilities

$$\tilde{\chi}_{\text{rpa}}^E = \tilde{\chi}_0^E + \tilde{\chi}_0^E \tilde{\chi}_{\text{rpa}}^E \quad (24)$$

$$\tilde{\chi}_{\text{tc}}^E = \tilde{P}^E + \tilde{P}^E \tilde{\chi}_{\text{tc}}^E \quad (25)$$

$$\tilde{\chi}_{\text{el}}^E = \tilde{\chi}_0^E + \tilde{\chi}_0^E \tilde{f}_{\text{Hxc}} \tilde{\chi}_{\text{el}}^E \quad (26)$$

that we use to define W^E (note that $\chi = v_c^{-\frac{1}{2}} \tilde{\chi} v_c^{-\frac{1}{2}}$, where χ and $\tilde{\chi}$ are unsymmetrized and symmetrized response functions):

$$W_{\text{rpa}}^E = v_c + v_c \chi_{\text{rpa}}^E v_c \quad (27)$$

$$W_{\text{tc}}^E = v_c + v_c \chi_{\text{tc}}^E v_c \quad (28)$$

$$W_{\text{el}}^E = f_{\text{Hxc}} + f_{\text{Hxc}} \chi_{\text{el}}^E f_{\text{Hxc}} \quad (29)$$

$$W_{\text{vel}}^E = v_c + f_{\text{Hxc}} \chi_{\text{el}}^E f_{\text{Hxc}} \quad (30)$$

To construct effective Hamiltonians beyond the RPA, one simply evaluates matrix elements of W^E defined in Eq. 28 - 30 on the active space, similar to Eq. 18. The evaluation of matrix elements of the bare Coulomb interaction is straightforward and can be performed using the standard Gygi-Baldereschi scheme.⁶³ The polarization component can be computed with a resolution-of-identity (RI) technique using the PDEP basis. We provide the detailed expression of the RI calculation in the SI, and we note again that the numerical accuracy of the matrix elements is controlled by the size of the PDEP basis N_{PDEP} .

3 Results

3.1 Computational setup

The calculations of effective Hamiltonians were carried out with the WEST code.⁴⁷ For calculations beyond the RPA, the exchange-correlation kernel f_{xc} was evaluated using a finite-field algorithm^{42,43} by coupling the WEST code with the Qbox code⁶⁴ in client-server mode. We used $N_{\text{PDEP}} = 512$ for the evaluation of the density response functions (Eq. 19), and convergence tests are presented in the SI. Kohn-Sham DFT orbitals were obtained with the Quantum Espresso code⁶⁵ and MLWFs with the Wannier90 code.⁶⁶ FCI calculations using effective Hamiltonians were performed with the PySCF code.⁶⁷

In our calculations we used plane-wave basis sets with a kinetic energy cutoff of 50/70 Ry in the calculations of spin-defects/SrTiO₃. The electron-ion interactions were represented by norm-conserving pseudopotentials from the SG15 library.⁶⁸ Spin-defects in diamond/4H-SiC were modeled with 216-atom/200-atom supercells. The SrTiO₃ solid was modeled with a 135-atom supercell. All calculations were performed with Γ -point sampling of the Brillouin zone, except the calculation of MLWFs for SrTiO₃, which was performed starting from non-self-consistent DFT calculations using a $4 \times 4 \times 4$ k-point mesh.

3.2 Calculation of environment dielectric screening beyond the RPA

We turn to discuss calculations of the environmental screened Coulomb interaction W^E beyond the RPA, using the different expressions presented in Sec. 2.2 to compute the excitation energies of several spin-defects in wide-gap semiconductors: the negatively charged nitrogen-vacancy (NV) center and the neutral silicon-vacancy (SiV) center in diamond, and the neutral divacancy (VV) and Cr impurity in 4H-SiC. These spin-defects are promising platforms for realizing solid-state quantum bits for quantum information processing, and they possess spin-triplet ground state and exhibit strongly-correlated electronic states that are critical for the initialization and read-out of their spin states.^{69–74} For instance, it has been shown that the majority of low-lying many-body electronic states of the NV center are strongly-correlated.^{75,76} We note that VV and Cr can exist in different configurations in the 4H-SiC lattice, and here we consider the hexagonal configurations. The atomistic structures of spin-defects are shown in Fig. 2.

To compute the excitation energies of spin-defects using the quantum embedding theory, we first carried out ground state spin-unrestricted DFT calculations using the PBE functional⁷⁷ to optimize the structure of these defects. Then we performed spin-restricted DFT calculations using the PBE and a dielectric dependent hybrid (DDH)^{78–83} functional to obtain mean-field descriptions of the electronic states, providing starting points for the construction of effective Hamiltonians. The fraction of exact exchange used in DDH calculations is taken as the inverse of the high-frequency dielectric constants ϵ_∞ , which is self-consistently determined to be 5.61/6.57 for diamond/silicon carbide; for comparison the experimental values for ϵ_∞ 5.70/6.52.⁸⁴ The spin restriction ensures that both spin channels are treated on an equal footing and the eigenstates of the resulting effective Hamiltonians are eigenstates of S^2 .^{4,85} In Fig. 3 we show the position of single-particle defect levels of spin-defects and the active spaces used to define the effective Hamiltonians. The active spaces are chosen to be sufficiently large to yield converged excitation energies of the spin-defects (see convergence

tests reported in Ref. 41,48). Using the effective Hamiltonians constructed with the quantum embedding theory, we performed FCI calculations⁸⁶ to compute the low-energy eigenstates and vertical excitation energies of spin-defects.

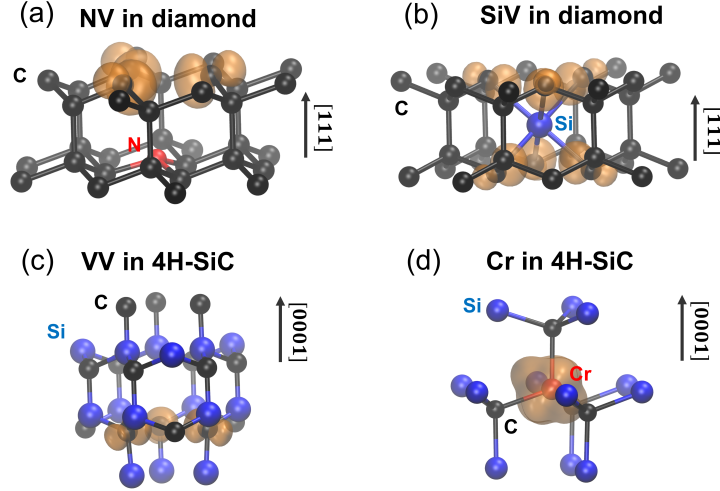


Figure 2: Structures and spin densities of the negatively-charged nitrogen-vacancy (NV) center in diamond (a), the neutral silicon-vacancy (SiV) center (b) in diamond, the neutral divacancy (VV) (*hh* configuration) in 4H-SiC (c) and the chromium (4+) impurity (*h* configuration) in 4H-SiC (d).

In Table 1 we present vertical excitation energies obtained from FCI calculations on effective Hamiltonians constructed using different expression of W^E (W_{rpa}^E , W_{tc}^E , W_{el}^E , W_{vel}^E) and with different DFT starting point (PBE, DDH). The W_{rpa}^E and W_{vel}^E results for NV and SiV were also reported in Ref. 41 and Ref. 48. As expected, excitation energies obtained using DDH starting points are significantly larger than those obtained using PBE, and DDH results are in better agreement with available reference values.⁴⁸ This comparison of DDH and PBE results is consistent with previous reports of Δ -SCF calculations of triplet excited states of NV and VV.⁷¹

Using calculations starting from Kohn-Sham eigenvalues and orbitals obtained with DDH functional, we obtain different results using different definitions of W^E . Compared to the results of cRPA calculations, calculations using W_{tc}^E and W_{el}^E lead to lower excitation energies while calculations using W_{vel}^E lead to higher excitation energies. These differences can

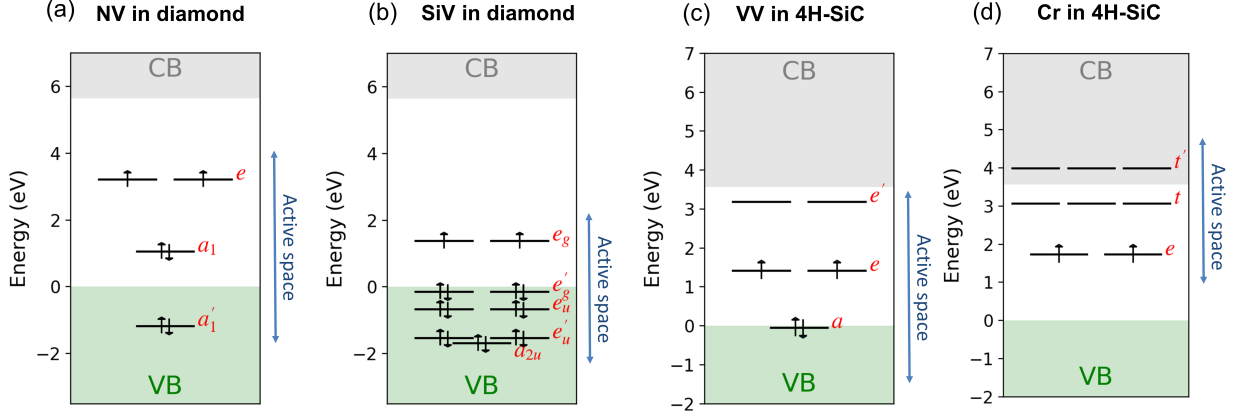


Figure 3: Defect levels obtained from spin-restricted DFT calculations using DDH functional for the negatively-charge nitrogen-vacancy (NV) center in diamond (a), the neutral silicon-vacancy (SiV) center (b) in diamond, the neutral divacancy (VV) in 4H-SiC (c) and the chromium (4+) impurity in 4H-SiC (d). Note that due to spin restriction, exchange splittings of defect levels in their spin triplet ground state are not reflected in these diagrams. The choice of active spaces for the NV and SiV centers is consistent with Ref. 41.

be understood by noticing that the exchange-correlation kernel f_{xc} tends to cancel out a small portion of the bare Coulomb interaction v . By inspecting Eq. 27-30, one can see that compared to the cRPA case, the cancellation of the bare Coulomb interaction and the exchange-correlation kernel leads to a smaller effective interaction W^E in the case of W_{tc}^E and W_{el}^E and a larger effective interaction in the case of W_{vel}^E .

By comparing the calculated excitation energies obtained with the DDH functional with experimental values, we find that using W_{vel}^E leads to best overall agreement. As an example, we discuss in detail the excitation energies between 1A_1 and 1E states of the NV center. Based on molecular orbital theory analysis,^{75,76} the $^1E \rightarrow ^1A_1$ excitation is a spin-flip transition of electrons in the e defect orbitals, and its excitation energy is approximately equal to twice the exchange integral $\langle e_x e_x | W^E | e_y e_y \rangle$, where e_x and e_y are the two degenerate e orbitals. Comparing the embedding theory results for excitation energies with the experimental zero phonon line (ZPL) value of 1.190 eV (which is a lower bound to the vertical excitation energy), we observe that embedding calculations using W_{rpa}^E (cRPA calculations) leads to an underestimation of the excitation energy (0.900 eV). Going beyond the RPA by

using W_{tc}^E and W_{el}^E leads to even more severe underestimations (0.471 eV and 0.824 eV). Instead, by properly accounting for the exchange-correlation effects between active space and environment, the excitation energy obtained with W_{vel}^E (1.198 eV) significantly reduces the underestimation of the cRPA result and leads to the best agreement with experiment. Similar trends are observed in the comparison of other calculated excitation energies with experiment, as summarized in Table 1.

Table 1: Vertical excitation energies (eV) of the negatively charged nitrogen vacancy (NV) center and neutral silicon vacancy (SiV) center in diamond, and the neutral divacancy (VV) and Cr impurity (4+) in 4H-SiC. DFT calculations were performed using the PBE and the DDH functional. Quantum embedding calculations were performed with different definitions of W^E (see text). Experimental measurements of zero phonon line (ZPL) energies are shown in brackets in the last column. Reference vertical excitation energies are computed from experimental ZPL when Stokes energies are available.

| System | Excitation | PBE | W_{tc}^E | W_{el}^E | W_{vel}^E | DDH | W_{tc}^E | W_{el}^E | W_{vel}^E | Previous works |
|--------|---|--------------------|------------|------------|--------------------|--------------------|------------|------------|--------------------|--|
| | | W_{rpa}^E | | | | W_{rpa}^E | | | | |
| NV | ${}^3E \leftrightarrow {}^3A_2$ | 1.395 ^a | 1.282 | 1.377 | 1.458 ^a | 1.921 ^b | 1.775 | 1.890 | 2.001 ^b | 2.180 ^c (1.945 ^c) |
| | ${}^1A_1 \leftrightarrow {}^3A_2$ | 1.211 ^a | 0.832 | 1.162 | 1.437 ^a | 1.376 ^b | 0.788 | 1.274 | 1.759 ^b | |
| | ${}^1E \leftrightarrow {}^3A_2$ | 0.396 ^a | 0.305 | 0.384 | 0.444 ^a | 0.476 ^b | 0.317 | 0.450 | 0.561 ^b | |
| | ${}^1A_1 \leftrightarrow {}^1E$ | 0.815 ^a | 0.527 | 0.778 | 0.993 ^a | 0.900 ^b | 0.471 | 0.824 | 1.198 ^b | |
| SiV | ${}^3E \leftrightarrow {}^1A_1$ | 0.184 ^a | 0.449 | 0.215 | 0.020 ^a | 0.545 ^b | 0.987 | 0.616 | 0.243 ^b | (1.190 ^d) (0.344-0.430 ^e) |
| | ${}^3E_u \leftrightarrow {}^3A_{2g}$ | 1.247 ^a | 1.263 | 1.244 | 1.258 ^a | 1.590 ^b | 1.623 | 1.586 | 1.594 ^b | |
| | ${}^1E_g \leftrightarrow {}^3A_{2g}$ | 0.232 ^a | 0.202 | 0.223 | 0.281 ^a | 0.261 ^b | 0.215 | 0.244 | 0.336 ^b | |
| | ${}^1A_{1g} \leftrightarrow {}^3A_{2g}$ | 0.404 ^a | 0.358 | 0.391 | 0.478 ^a | 0.466 ^b | 0.393 | 0.440 | 0.583 ^b | |
| VV | ${}^1A_{1u} \leftrightarrow {}^3A_{2g}$ | 1.262 ^a | 1.265 | 1.258 | 1.277 ^a | 1.608 ^b | 1.617 | 1.602 | 1.623 ^b | 1.240 ^h (1.094 ⁱ) |
| | ${}^3E \leftrightarrow {}^3A_2$ | 0.962 | 0.881 | 0.957 | 0.985 | 1.231 | 1.109 | 1.220 | 1.270 | |
| | ${}^1A_1 \leftrightarrow {}^3A_2$ | 0.776 | 0.483 | 0.756 | 0.908 | 0.921 | 0.429 | 0.875 | 1.156 | |
| | ${}^1E \leftrightarrow {}^3A_2$ | 0.246 | 0.176 | 0.242 | 0.274 | 0.299 | 0.169 | 0.288 | 0.348 | |
| Cr | ${}^1A_1 \leftrightarrow {}^1E$ | 0.530 | 0.308 | 0.515 | 0.634 | 0.622 | 0.260 | 0.587 | 0.808 | (1.190 ^j) |
| | ${}^3E \leftrightarrow {}^1A_1$ | 0.186 | 0.398 | 0.201 | 0.077 | 0.310 | 0.680 | 0.345 | 0.114 | |
| | ${}^3E \leftrightarrow {}^3A_2$ | 0.931 | 0.984 | 0.931 | 0.890 | 1.468 | 1.587 | 1.534 | 1.343 | |
| | ${}^3A_1 \leftrightarrow {}^3A_2$ | 1.002 | 1.072 | 1.011 | 0.956 | 1.527 | 1.664 | 1.602 | 1.394 | |
| | ${}^3E' \leftrightarrow {}^3A_2$ | 1.134 | 1.122 | 1.073 | 1.189 | 1.769 | 1.760 | 1.705 | 1.744 | |
| | ${}^3A_2' \leftrightarrow {}^3A_2$ | 1.177 | 1.153 | 1.106 | 1.237 | 1.805 | 1.794 | 1.731 | 1.783 | |
| | ${}^1E \leftrightarrow {}^3A_2$ | 0.902 | 0.854 | 0.828 | 1.017 | 1.097 | 1.075 | 1.073 | 1.130 | |
| | ${}^1A_1 \leftrightarrow {}^3A_2$ | 1.467 | 1.366 | 1.374 | 1.566 | 1.992 | 1.873 | 1.819 | 2.013 | |

^aRef 48. ^bRef 41. ^cRef 87. ^dRef 88. ^eEstimated by Ref 89 using a model for intersystem crossing. ^fComputed using Stokes energy from Ref 90. ^gRef 91. ^hComputed using Stokes energy from Ref 4. ⁱRef 92. ^jRef 93.

3.3 Calculation of environment dielectric screening with general active spaces

We now present two proof-of-principles examples of quantum embedding calculations using general active spaces.

In the first example, we compute the vertical excitation energies of the NV center in diamond using a minimum active space composed of 4 Kohn-Sham orbitals a'_1 , a_1 , e_x , and e_y . We performed quantum embedding calculations both by directly using the 4 Kohn-Sham orbitals and by using 4 MLWFs computed from the Kohn-Sham orbitals. The resulting excitation energies for the many-body $^1E/{}^1A_1/{}^3E$ states are 0.485/1.364/1.977 eV at the cRPA level if evaluated using Kohn-Sham orbitals and 0.485/1.364/1.976 eV if evaluated using MLWFs (beyond-RPA results show similar agreement). The excellent agreement between results obtained using the two different active spaces serves as a validation of the formalism and implementation.

In the second example, we apply the quantum embedding theory to compute the Hubbard U and J parameters entering DFT+ U calculations.³ Hubbard parameters can be computed as the average values of certain matrix elements in the effective Hamiltonian, and the cRPA approach has been extensively used for first-principles predictions of these parameters for solids containing transition metal ions.^{28,33–36,94,95}

Here we apply the quantum embedding theory to compute the Hubbard- U and Hubbard- J parameters for the Ti t_{2g} orbitals of SrTiO_3 . We first perform ground state DFT calculations of SrTiO_3 using the PBE functional to obtain the eigenstates of the Kohn-Sham Hamiltonian. Then we construct effective Hamiltonians where the active space is composed of the three MLWFs that correspond to the t_{2g} orbitals of Ti (see SI). This choice of active space corresponds to the $t_{2g} - t_{2g}$ model of SrTiO_3 often considered in literature.⁹⁶ The Hubbard parameters can then be computed as $U = \frac{1}{3} \sum_{i=1}^3 W_{iii}^E$ and $J = \frac{1}{6} \sum_{i,j=1, i \neq j}^3 W_{ijji}^E$.

Quantum embedding calculations at the RPA level predict the Hubbard U/J parameters to be 3.90/0.58 eV, in good agreement with previous cRPA calculations (3.76/0.46 eV for

U/J).⁹⁷ The small differences are attributed to different choices of the pseudopotentials and Brillouin zone sampling. The Hubbard-J parameters are found to be rather insensitive to the choice of W^E (0.58/0.58/0.58/0.59 eV for $W_{\text{rpa}}^E/W_{\text{tc}}^E/W_{\text{el}}^E/W_{\text{vel}}^E$), as opposed to the Hubbard-U parameters (3.90/3.58/3.87/4.37 eV for $W_{\text{rpa}}^E/W_{\text{tc}}^E/W_{\text{el}}^E/W_{\text{vel}}^E$). We note that calculations using W_{tc}^E and W_{el}^E yield smaller values of U (3.58 eV and 3.87 eV), while calculations using W_{vel}^E a larger value (4.37 eV), consistent with the trend observed for the excitation energies of spin-defects as discussed in Sec. 3.2.

In order to assess the impact of the Hubbard parameters predicted by the embedding theory on the electronic structure of SrTiO_3 , we performed DFT+U calculations to obtain the band gap of SrTiO_3 . The experimental (indirect) band gap is 3.25 eV and the PBE prediction is 1.93 eV. The DFT+U calculations using Hubbard-U parameters with $W_{\text{rpa}}^E/W_{\text{tc}}^E/W_{\text{el}}^E/W_{\text{vel}}^E$ lead to band gaps of 2.25/2.22/2.25/2.30 eV, i.e. to values rather similar to each other. Although DFT+U calculations do not yield band gaps in quantitative agreement with experimental band gap due to covalent effects,⁹⁸ using W_{vel}^E as the effective electron-electron interaction leads to slight improvement in the predicted gap value.

4 Conclusions

In summary, in this work we presented a detailed derivation of the quantum embedding theory recently introduced in Ref. 41, and we generalized the formulation to active spaces defined using orbitals that are not eigenstates of the Kohn-Sham Hamiltonian. In addition, we discussed different approaches to compute the dielectric screening beyond the random phase approximation, which we applied to spin defects in semiconductors. In particular, we presented a physically motivated choice of the definition of screened Coulomb interaction, which turns out to yield the best agreement with experiments for excitation energies. Finally, using NV center in diamond and the SrTiO_3 solid as examples, we demonstrate how quantum embedding calculations may be performed using general active spaces composed of localized

orbitals.

We note that one of the possible advantages of using MLWFs instead of eigenstates is the ability to define active spaces associated to specific regions of the material, which can then be treated at different levels of theory. For example consider a nanocomposite (e.g. a nanoparticle in a matrix or in a solvent) or solvated ions or molecules in water. We may associate MLWFs to the nanoparticle or to the solute and its solvation shell, in order to define an active space and consider electronic excitations within that active space. The embedding theory is then used to properly take into account matrix or solvation effects.

Our work paves the way to the application of the quantum embedding theory to challenging chemical and materials science problems, which may be solved using effective Hamiltonians on classical and near-term quantum computers.

Acknowledgements

This work was supported by MICCoM, as part of the Computational Materials Sciences Program funded by the U.S. Department of Energy, Office of Science, Basic Energy Sciences, Materials Sciences and Engineering Division through Argonne National Laboratory, under contract number DE-AC02-06CH11357. This research used resources of the National Energy Research Scientific Computing Center (NERSC), a DOE Office of Science User Facility supported by the Office of Science of the US Department of Energy under Contract No. DE-AC02-05CH11231, and resources of the University of Chicago Research Computing Center.

References

- (1) Cohen, A. J.; Mori-Sánchez, P.; Yang, W. Insights into current limitations of density functional theory. *Science* **2008**, *321*, 792–794.
- (2) Su, N. Q.; Li, C.; Yang, W. Describing strong correlation with fractional-spin correction in density functional theory. *Proc. Natl. Acad. Sci. U. S. A.* **2018**, *115*, 9678–9683.
- (3) Anisimov, V. I.; Aryasetiawan, F.; Lichtenstein, A. First-principles calculations of the electronic structure and spectra of strongly correlated systems: the LDA+ U method. *J. Phys.: Condens. Matter* **1997**, *9*, 767.
- (4) Bockstedte, M.; Schütz, F.; Garratt, T.; Ivády, V.; Gali, A. Ab initio description of highly correlated states in defects for realizing quantum bits. *npj Quantum Mater.* **2018**, *3*, 31.
- (5) Kurashige, Y.; Chan, G. K.-L.; Yanai, T. Entangled quantum electronic wavefunctions of the Mn₄CaO₅ cluster in photosystem II. *Nat. Chem.* **2013**, *5*, 660–666.
- (6) Sharma, S.; Sivalingam, K.; Neese, F.; Chan, G. K.-L. Low-energy spectrum of iron–sulfur clusters directly from many-particle quantum mechanics. *Nat. Chem.* **2014**, *6*, 927–933.
- (7) Georges, A.; Kotliar, G.; Krauth, W.; Rozenberg, M. J. Dynamical mean-field theory of strongly correlated fermion systems and the limit of infinite dimensions. *Rev. Mod. Phys.* **1996**, *68*, 13–125.
- (8) Kotliar, G.; Savrasov, S. Y.; Haule, K.; Oudovenko, V. S.; Parcollet, O.; Marianetti, C. A. Electronic structure calculations with dynamical mean-field theory. *Rev. Mod. Phys.* **2006**, *78*, 865–951.
- (9) Ceperley, D.; Alder, B. Quantum Monte Carlo. *Science* **1986**, *231*, 555–560.

- (10) Wagner, L. K.; Ceperley, D. M. Discovering correlated fermions using quantum Monte Carlo. *Rep. Prog. Phys.* **2016**, *79*, 094501.
- (11) Lischka, H.; Nachtigallova, D.; Aquino, A. J. A.; Szalay, P. G.; Plasser, F.; Machado, F. B. C.; Barbatti, M. Multireference Approaches for Excited States of Molecules. *Chem. Rev.* **2018**, *118*, 7293–7361.
- (12) Sun, Q.; Chan, G. K.-L. Quantum Embedding Theories. *Acc. Chem. Res.* **2016**, *49*, 2705–2712.
- (13) Huang, P.; Carter, E. A. Self-consistent embedding theory for locally correlated configuration interaction wave functions in condensed matter. *J. Chem. Phys.* **2006**, *125*, 084102.
- (14) Huang, C.; Pavone, M.; Carter, E. A. Quantum mechanical embedding theory based on a unique embedding potential. *J. Chem. Phys.* **2011**, *134*, 154110.
- (15) Goodpaster, J. D.; Barnes, T. A.; Manby, F. R.; Miller, T. F. Accurate and systematically improvable density functional theory embedding for correlated wavefunctions. *J. Chem. Phys.* **2014**, *140*, 18A507.
- (16) Jacob, C. R.; Neugebauer, J. Subsystem density-functional theory. *Wiley Interdiscip. Rev.: Comput. Mol. Sci.* **2014**, *4*, 325–362.
- (17) Genova, A.; Ceresoli, D.; Pavanello, M. Periodic subsystem density-functional theory. *J. Chem. Phys.* **2014**, *141*, 174101.
- (18) Wen, X.; Graham, D. S.; Chulhai, D. V.; Goodpaster, J. D. Absolutely Localized Projection-Based Embedding for Excited States. *J. Chem. Theory Comput.* **2019**, *16*, 385–398.
- (19) Knizia, G.; Chan, G. K.-L. Density Matrix Embedding: A Simple Alternative to Dynamical Mean-Field Theory. *Phys. Rev. Lett.* **2012**, *109*, 186404.

- (20) Wouters, S.; Jiménez-Hoyos, C. A.; Sun, Q.; Chan, G. K.-L. A Practical Guide to Density Matrix Embedding Theory in Quantum Chemistry. *J. Chem. Theory Comput.* **2016**, *12*, 2706–2719.
- (21) Pham, H. Q.; Hermes, M. R.; Gagliardi, L. Periodic Electronic Structure Calculations with the Density Matrix Embedding Theory. *J. Chem. Theory Comput.* **2019**, *16*, 130–140.
- (22) Lan, T. N.; Kananenka, A. A.; Zgid, D. Rigorous Ab Initio Quantum Embedding for Quantum Chemistry Using Green’s Function Theory: Screened Interaction, Nonlocal Self-Energy Relaxation, Orbital Basis, and Chemical Accuracy. *J. Chem. Theory Comput.* **2016**, *12*, 4856–4870.
- (23) Dvorak, M.; Rinke, P. Dynamical configuration interaction: Quantum embedding that combines wave functions and Green’s functions. *Phys. Rev. B* **2019**, *99*, 115134.
- (24) Zhu, T.; Jiménez-Hoyos, C. A.; McClain, J.; Berkelbach, T. C.; Chan, G. K.-L. Coupled-cluster impurity solvers for dynamical mean-field theory. *Physical Review B* **2019**, *100*, 115154.
- (25) Aryasetiawan, F.; Imada, M.; Georges, A.; Kotliar, G.; Biermann, S.; Lichtenstein, A. I. Frequency-dependent local interactions and low-energy effective models from electronic structure calculations. *Phys. Rev. B* **2004**, *70*, 195104.
- (26) Aryasetiawan, F.; Tomczak, J. M.; Miyake, T.; Sakuma, R. Downfolded Self-Energy of Many-Electron Systems. *Phys. Rev. Lett.* **2009**, *102*.
- (27) Miyake, T.; Aryasetiawan, F.; Imada, M. Ab initio procedure for constructing effective models of correlated materials with entangled band structure. *Phys. Rev. B* **2009**, *80*, 155134.

- (28) Imada, M.; Miyake, T. Electronic Structure Calculation by First Principles for Strongly Correlated Electron Systems. *J. Phys. Soc. Jpn.* **2010**, *79*, 112001.
- (29) Hirayama, M.; Miyake, T.; Imada, M. Derivation of static low-energy effective models by an ab initio downfolding method without double counting of Coulomb correlations: Application to SrVO_3 , FeSe , and FeTe . *Phys. Rev. B* **2013**, *87*, 195144.
- (30) Hirayama, M.; Miyake, T.; Imada, M.; Biermann, S. Low-energy effective Hamiltonians for correlated electron systems beyond density functional theory. *Phys. Rev. B* **2017**, *96*, 075102.
- (31) Cho, Y.; Berkelbach, T. C. Environmentally sensitive theory of electronic and optical transitions in atomically thin semiconductors. *Phys. Rev. B* **2018**, *97*, 041409.
- (32) Romanova, M.; Vlček, V. Decomposition and embedding in the stochastic GW self-energy. *J. Chem. Phys.* **2020**, *153*, 134103.
- (33) Aryasetiawan, F.; Karlsson, K.; Jepsen, O.; Schönberger, U. Calculations of Hubbard U from first-principles. *Phys. Rev. B* **2006**, *74*.
- (34) Shih, B.-C.; Zhang, Y.; Zhang, W.; Zhang, P. Screened Coulomb interaction of localized electrons in solids from first principles. *Phys. Rev. B* **2012**, *85*.
- (35) Nilsson, F.; Aryasetiawan, F. Electronic structure of strongly correlated materials: from one-particle to many-body theory. *Mater. Res. Express* **2017**, *4*, 034001.
- (36) Tadano, T.; Nomura, Y.; Imada, M. Ab initio derivation of an effective Hamiltonian for the $\text{La}_2\text{CuO}_4/\text{La}_{1.55}\text{Sr}_{0.45}\text{CuO}_4$ heterostructure. *Phys. Rev. B* **2019**, *99*, 155148.
- (37) Wehling, T. O.; Şaşıoğlu, E.; Friedrich, C.; Lichtenstein, A. I.; Katsnelson, M. I.; Blügel, S. Strength of Effective Coulomb Interactions in Graphene and Graphite. *Phys. Rev. Lett.* **2011**, *106*, 236805.

- (38) Honerkamp, C.; Shinaoka, H.; Assaad, F. F.; Werner, P. Limitations of constrained random phase approximation downfolding. *Phys. Rev. B* **2018**, *98*, 235151.
- (39) Adler, S. L. Quantum Theory of the Dielectric Constant in Real Solids. *Phys. Rev.* **1962**, *126*, 413–420.
- (40) Wiser, N. Dielectric Constant with Local Field Effects Included. *Phys. Rev.* **1963**, *129*, 62–69.
- (41) Ma, H.; Govoni, M.; Galli, G. Quantum simulations of materials on near-term quantum computers. *npj Comput. Mater.* **2020**, *6*, 85.
- (42) Ma, H.; Govoni, M.; Gygi, F.; Galli, G. A Finite-Field Approach for GW Calculations beyond the Random Phase Approximation. *J. Chem. Theory Comput.* **2018**, *15*, 154–164.
- (43) Nguyen, N. L.; Ma, H.; Govoni, M.; Gygi, F.; Galli, G. Finite-Field Approach to Solving the Bethe-Salpeter Equation. *Phys. Rev. Lett.* **2019**, *122*, 237402.
- (44) Wilson, H. F.; Gygi, F.; Galli, G. Efficient iterative method for calculations of dielectric matrices. *Phys. Rev. B* **2008**, *78*, 113303.
- (45) Nguyen, H.-V.; Pham, T. A.; Rocca, D.; Galli, G. Improving accuracy and efficiency of calculations of photoemission spectra within the many-body perturbation theory. *Phys. Rev. B* **2012**, *85*, 081101.
- (46) Pham, T. A.; Nguyen, H.-V.; Rocca, D.; Galli, G. GW calculations using the spectral decomposition of the dielectric matrix: Verification, validation, and comparison of methods. *Phys. Rev. B* **2013**, *87*, 155148.
- (47) Govoni, M.; Galli, G. Large Scale GW Calculations. *J. Chem. Theory Comput.* **2015**, *11*, 2680–2696.

- (48) Ma, H.; Sheng, N.; Govoni, M.; Galli, G. First-principles studies of strongly correlated states in defect spin qubits in diamond. *Phys. Chem. Chem. Phys.* **2020**,
- (49) Marzari, N.; Mostofi, A. A.; Yates, J. R.; Souza, I.; Vanderbilt, D. Maximally localized Wannier functions: Theory and applications. *Rev. Mod. Phys.* **2012**, *84*, 1419.
- (50) Timrov, I.; Marzari, N.; Cococcioni, M. Hubbard parameters from density-functional perturbation theory. *Phys. Rev. B* **2018**, *98*, 085127.
- (51) Hedin, L. New Method for Calculating the One-Particle Green’s Function with Application to the Electron-Gas Problem. *Phys. Rev.* **1965**, *139*, A796–A823.
- (52) Some literatures define χ_0^A by adding O^A to all the four appearances of Kohn-Sham orbitals in Eq. 7. This definition is equivalent to our definition if the active space is spanned by a set of Kohn-Sham orbitals. For general active spaces, we tested quantum embedding calculations using both definitions and we found the difference in results (e.g. Hubbard parameters of SrTiO₃) is negligible.
- (53) Liechtenstein, A. I.; Anisimov, V. I.; Zaanen, J. Density-functional theory and strong interactions: Orbital ordering in Mott-Hubbard insulators. *Phys. Rev. B* **1995**, *52*, R5467–R5470.
- (54) Ryee, S.; Han, M. J. The effect of double counting, spin density, and Hund interaction in the different DFT+ U functionals. *Sci. Rep.* **2018**, *8*, 1–11.
- (55) In principle, one can also define an electron-test-charge screened Coulomb interaction W_{etc} that represents the screened interaction between a test charge and an electron. However, it is difficult to apply the cRPA-type treatment to W_{etc} and define a partially screened interaction because it is difficult to write W_{etc} in the form of a Dyson-like equation, so we will not consider W_{etc} in this work.

- (56) Hybertsen, M. S.; Louie, S. G. Electron correlation in semiconductors and insulators: Band gaps and quasiparticle energies. *Phys. Rev. B* **1986**, *34*, 5390.
- (57) Sole, R. D.; Reining, L.; Godby, R. W. GWT approximation for electron self-energies in semiconductors and insulators. *Phys. Rev. B* **1994**, *49*, 8024–8028.
- (58) Martin, R. M.; Reining, L.; Ceperley, D. M. *Interacting Electrons: Theory and Computational Approaches*; Cambridge University Press, 2016.
- (59) Paier, J.; Marsman, M.; Kresse, G. Dielectric properties and excitons for extended systems from hybrid functionals. *Phys. Rev. B* **2008**, *78*, 121201.
- (60) Grüneis, A.; Kresse, G.; Hinuma, Y.; Oba, F. Ionization Potentials of Solids: The Importance of Vertex Corrections. *Phys. Rev. Lett.* **2014**, *112*, 096401.
- (61) McAvoy, R. L.; Govoni, M.; Galli, G. Coupling First-Principles Calculations of Electron–Electron and Electron–Phonon Scattering, and Applications to Carbon-Based Nanostructures. *J. Chem. Theory Comput.* **2018**, *14*, 6269–6275.
- (62) Giustino, F. Electron-phonon interactions from first principles. *Rev. Mod. Phys.* **2017**, *89*, 015003.
- (63) Gygi, F.; Baldereschi, A. Self-consistent Hartree-Fock and screened-exchange calculations in solids: Application to silicon. *Phys. Rev. B* **1986**, *34*, 4405–4408.
- (64) Gygi, F. Architecture of Qbox: A scalable first-principles molecular dynamics code. *IBM J. Res. Dev.* **2008**, *52*, 137–144.
- (65) Giannozzi, P.; Baroni, S.; Bonini, N.; Calandra, M.; Car, R.; Cavazzoni, C.; Ceresoli, D.; Chiarotti, G. L.; Cococcioni, M.; Dabo, I.; Corso, A. D.; de Gironcoli, S.; Fabris, S.; Fratesi, G.; Gebauer, R.; Gerstmann, U.; Gougoussis, C.; Kokalj, A.; Lazzeri, M.; Martin-Samos, L.; Marzari, N.; Mauri, F.; Mazzarello, R.; Paolini, S.; Pasquarello, A.; Paulatto, L.; Sbraccia, C.; Scandolo, S.; Sclauzero, G.; Seitsonen, A. P.; Smogunov, A.;

- Umari, P.; Wentzcovitch, R. M. QUANTUM ESPRESSO: a modular and open-source software project for quantum simulations of materials. *J. Phys.: Condens. Matter* **2009**, *21*, 395502.
- (66) Mostofi, A. A.; Yates, J. R.; Lee, Y.-S.; Souza, I.; Vanderbilt, D.; Marzari, N. wannier90: A tool for obtaining maximally-localised Wannier functions. *Comput. Phys. Commun.* **2008**, *178*, 685–699.
- (67) Sun, Q.; Berkelbach, T. C.; Blunt, N. S.; Booth, G. H.; Guo, S.; Li, Z.; Liu, J.; McClain, J. D.; Sayfutyarova, E. R.; Sharma, S.; Wouters, S.; Chan, G. K.-L. Py SCF: the Python-based simulations of chemistry framework. *Wiley Interdiscip. Rev.: Comput. Mol. Sci.* **2017**, *8*, e1340.
- (68) Schlipf, M.; Gygi, F. Optimization algorithm for the generation of ONCV pseudopotentials. *Comput. Phys. Commun.* **2015**, *196*, 36–44.
- (69) Weber, J. R.; Koehl, W. F.; Varley, J. B.; Janotti, A.; Buckley, B. B.; de Walle, C. G. V.; Awschalom, D. D. Quantum computing with defects. *Proc. Natl. Acad. Sci. U. S. A.* **2010**, *107*, 8513–8518.
- (70) Seo, H.; Govoni, M.; Galli, G. Design of defect spins in piezoelectric aluminum nitride for solid-state hybrid quantum technologies. *Sci. Rep.* **2016**, *6*, 20803.
- (71) Seo, H.; Ma, H.; Govoni, M.; Galli, G. Designing defect-based qubit candidates in wide-gap binary semiconductors for solid-state quantum technologies. *Phys. Rev. Mater.* **2017**, *1*, 075002.
- (72) Ivády, V.; Abrikosov, I. A.; Gali, A. First principles calculation of spin-related quantities for point defect qubit research. *npj Comput. Mater.* **2018**, *4*.
- (73) Dreyer, C. E.; Alkauskas, A.; Lyons, J. L.; Janotti, A.; Van de Walle, C. G. First-

- Principles Calculations of Point Defects for Quantum Technologies. *Annu. Rev. Mater. Res.* **2018**, *48*, 1–26.
- (74) Anderson, C. P.; Bourassa, A.; Miao, K. C.; Wolfowicz, G.; Mintun, P. J.; Crook, A. L.; Abe, H.; Ul Hassan, J.; Son, N. T.; Ohshima, T.; Awschalom, D. D. Electrical and optical control of single spins integrated in scalable semiconductor devices. *Science* **2019**, *366*, 1225–1230.
- (75) Maze, J. R.; Gali, A.; Togan, E.; Chu, Y.; Trifonov, A.; Kaxiras, E.; Lukin, M. D. Properties of nitrogen-vacancy centers in diamond: the group theoretic approach. *New J. Phys.* **2011**, *13*, 025025.
- (76) Doherty, M. W.; Manson, N. B.; Delaney, P.; Hollenberg, L. C. L. The negatively charged nitrogen-vacancy centre in diamond: the electronic solution. *New J. Phys.* **2011**, *13*, 025019.
- (77) Perdew, J. P.; Burke, K.; Ernzerhof, M. Generalized Gradient Approximation Made Simple. *Phys. Rev. Lett.* **1996**, *77*, 3865–3868.
- (78) Skone, J. H.; Govoni, M.; Galli, G. Self-consistent hybrid functional for condensed systems. *Phys. Rev. B* **2014**, *89*, 195112.
- (79) Skone, J. H.; Govoni, M.; Galli, G. Nonempirical range-separated hybrid functionals for solids and molecules. *Phys. Rev. B* **2016**, *93*, 235106.
- (80) Brawand, N. P.; Vörös, M.; Govoni, M.; Galli, G. Generalization of Dielectric-Dependent Hybrid Functionals to Finite Systems. *Phys. Rev. X* **2016**, *6*, 041002.
- (81) Brawand, N. P.; Govoni, M.; Vörös, M.; Galli, G. Performance and Self-Consistency of the Generalized Dielectric Dependent Hybrid Functional. *J. Chem. Theory Comput.* **2017**, *13*, 3318–3325, PMID: 28537727.

- (82) Gerosa, M.; Bottani, C. E.; Valentin, C. D.; Onida, G.; Pacchioni, G. Accuracy of dielectric-dependent hybrid functionals in the prediction of optoelectronic properties of metal oxide semiconductors: a comprehensive comparison with many-body GW and experiments. *J. Phys.: Condens. Matter* **2017**, *30*, 044003.
- (83) Zheng, H.; Govoni, M.; Galli, G. Dielectric-dependent hybrid functionals for heterogeneous materials. *Phys. Rev. Materials* **2019**, *3*, 073803.
- (84) Cardona, M.; Peter, Y. Y. *Fundamentals of semiconductors*; Springer, 2005.
- (85) Ivády, V.; Barcza, G.; Thiering, G.; Li, S.; Hamdi, H.; Chou, J.-P.; Legeza, Ö.; Gali, A. Ab initio theory of the negatively charged boron vacancy qubit in hexagonal boron nitride. *Npj Comput. Mater.* **2020**, *6*, 1–6.
- (86) Knowles, P.; Handy, N. A new determinant-based full configuration interaction method. *Chem. Phys. Lett.* **1984**, *111*, 315–321.
- (87) Davies, G.; Hamer, M. F. Optical Studies of the 1.945 eV Vibronic Band in Diamond. *Proc. R. Soc. A* **1976**, *348*, 285–298.
- (88) Rogers, L. J.; Armstrong, S.; Sellars, M. J.; Manson, N. B. Infrared emission of the NV centre in diamond: Zeeman and uniaxial stress studies. *New J. Phys.* **2008**, *10*, 103024.
- (89) Goldman, M. L.; Doherty, M. W.; Sipahigil, A.; Yao, N. Y.; Bennett, S. D.; Manson, N. B.; Kubanek, A.; Lukin, M. D. State-selective intersystem crossing in nitrogen-vacancy centers. *Phys. Rev. B* **2015**, *91*, 165201.
- (90) Thiering, G.; Gali, A. The $(eg \otimes eu) \otimes Eg$ product Jahn–Teller effect in the neutral group-IV vacancy quantum bits in diamond. *npj Comput. Mater.* **2019**, *5*, 18.
- (91) Green, B. L.; Doherty, M. W.; Nako, E.; Manson, N. B.; D’Haenens-Johansson, U. F. S.; Williams, S. D.; Twitchen, D. J.; Newton, M. E. Electronic structure of the neutral silicon-vacancy center in diamond. *Phys. Rev. B* **2019**, *99*, 161112.

- (92) Koehl, W. F.; Buckley, B. B.; Heremans, F. J.; Calusine, G.; Awschalom, D. D. Room temperature coherent control of defect spin qubits in silicon carbide. *Nature* **2011**, *479*, 84–87.
- (93) Son, N. T.; Ellison, A.; Magnusson, B.; MacMillan, M. F.; Chen, W. M.; Monemar, B.; Janzén, E. Photoluminescence and Zeeman effect in chromium-doped 4H and 6H SiC. *J. Appl. Phys.* **1999**, *86*, 4348–4353.
- (94) Solovyev, I. V.; Imada, M. Screening of Coulomb interactions in transition metals. *Phys. Rev. B* **2005**, *71*.
- (95) Karlsson, K.; Aryasetiawan, F.; Jepsen, O. Method for calculating the electronic structure of correlated materials from a truly first-principles LDA+ U scheme. *Phys. Rev. B* **2010**, *81*, 245113.
- (96) Vaugier, L.; Jiang, H.; Biermann, S. Hubbard U and Hund exchange J in transition metal oxides: Screening versus localization trends from constrained random phase approximation. *Phys. Rev. B* **2012**, *86*, 165105.
- (97) Hirayama, M.; Miyake, T.; Imada, M. Ab initio Low-energy model of transition-metal-oxide heterostructure $\text{LaAlO}_3/\text{SrTiO}_3$. *J. Phys. Soc. Jpn.* **2012**, *81*, 084708.
- (98) Ricca, C.; Timrov, I.; Cococcioni, M.; Marzari, N.; Aschauer, U. Self-consistent DFT + U + V study of oxygen vacancies in SrTiO_3 . *Phys. Rev. Research* **2020**, *2*, 023313.